



# Analytical Prediction of the Shear Behaviour of Rock Joints with Quantified Waviness and Unevenness Through Wavelet Analysis

Yingchun Li<sup>1</sup> · Shengyue Sun<sup>1</sup> · Chun'an Tang<sup>1</sup>

Received: 12 September 2018 / Accepted: 6 April 2019 / Published online: 20 April 2019  
 © Springer-Verlag GmbH Austria, part of Springer Nature 2019

## Abstract

We present an analytical model for the shear behaviour of a rock joint with waviness and unevenness. The waviness and unevenness of a natural joint profile are quantitatively separated through wavelet analysis. The critical waviness and critical unevenness of a joint profile are subsequently determined. The degradation process of each-order asperity is predicted by considering the role of plastic tangential work in shear, by which the sheared-off asperity area and the dilation angle are quantified. Both the dilation angles of critical waviness and critical unevenness decay, as plastic tangential work accumulates. The analytical predictions are compared with the experimental data from direct shear tests on both regular- and irregular-shaped joints. Good agreement between analytical predictions and laboratory-measured curves demonstrates the capability of the developed model. Therefore, the model is capable of assessing the stability of rock-engineering structures with ubiquitous joints.

**Keywords** Rock joint · Waviness and unevenness · Wavelet analysis · Dilation and degradation

## List of Symbols

$A_u$	Amplitude of critical unevenness	$S_w^0$	Initial area of critical waviness
$A_w$	Amplitude of critical waviness	$S_u$	Unsheared area of critical unevenness
$A_u^0$	Initial amplitude of critical unevenness	$S_u^b$	Area of critical unevenness base
$A_w^0$	Initial amplitude of critical waviness	$S_u^s$	Sheared area of critical unevenness
$a_s$	Sheared area ratio	$S_w$	Unsheared area of critical waviness
$a_u^s$	Sheared area ratio of critical unevenness	$S_w^b$	Area of critical waviness base
$a_w^s$	Sheared area ratio of critical waviness	$S_w^s$	Sheared area of critical waviness
$c_u$	Degradation coefficient of critical unevenness	$W_e^s$	Elastic tangential energy
$c_w$	Degradation coefficient of critical waviness	$W_s^p$	Plastic tangential work
$dS_u^s$	Increment of the sheared area of critical unevenness	$\alpha_0$	Initial inclination angle of critical unevenness
$dW_s^p$	Increment of plastic tangential work	$\alpha_m^d$	Mobilisable dilation angle of critical unevenness
$d\tau$	Increment of shear stress	$\delta_{ave}$	Average percent error
$F$	Reduction factor	$\delta_{ave}(\delta_n)$	Average percent error of dilation
$i_0$	Initial inclination angle of critical waviness	$\delta_{ave}(\tau)$	Average percent error of shear stress
$i_d$	Dilation angle of critical waviness	$\delta_n^{pre}$	Predicted dilation
$i_d^m$	Mobilisable dilation angle of critical waviness	$\delta_n^{exp}$	Experimental dilation
$K$	Dimensionless coefficient	$\delta_{ms}^e$	Maximum elastic shear displacement
$k_s$	Joint shear stiffness	$\delta_s^e$	Elastic shear displacement
$S_u^0$	Initial area of critical unevenness	$\delta_s^p$	Plastic shear displacement
		$\delta_n$	Joint dilation
		$\Delta\delta_n$	Incremental dilation
		$\Delta\delta_s^p$	Plastic shear displacement increment
		$\lambda_u$	Wavelength of critical unevenness
		$\lambda_u^0$	Initial wavelength of critical unevenness
		$\lambda_w$	Wavelength of critical waviness
		$\lambda_w^0$	Initial wavelength of critical waviness

✉ Yingchun Li  
 yingchun\_li@dlut.edu.cn

<sup>1</sup> State Key Laboratory of Coastal and Offshore Engineering, Dalian University of Technology, Dalian 116024, China

$\sigma_c$	Uniaxial compressive strength of rock
$\sigma_n$	Normal stress
$\sigma_T^n$	Transitional normal stress
$\sigma_T^s$	Transitional shear stress
$\tau$	Shear stress
$\tau_b$	Basic frictional strength
$\tau_m$	Mobilisable shear strength
$\tau^{\text{exp}}$	Experimental shear stress
$\tau_{\text{pre}}$	Predicted shear stress
$\phi_b$	Basic friction angle

## 1 Introduction

The stability of natural and engineering rock structures, such as rock slopes and underground excavations, is largely affected by the presence of rock joints along which slide failure can easily take place. Natural joints possess two-order roughness, i.e., waviness (first-order) and unevenness (second-order). Both order asperities experience dilation and degradation, leading to the non-linear mechanical response of a rock joint to shear loading. Quantifying the evolution of waviness and unevenness is crucial to constitute an adequate model for simulating the shear behaviour of a rock joint.

The mechanical reaction of a rock joint to shear mainly depends on normal stress, rock properties, and surface roughness (Patton 1966; Ladanyi and Archambault 1969; Barton 1973). When the normal stress is low, the rock joint fails due to the slide of asperities against each other. Under this circumstance, dilation dominates the mode of shear failure. If the normal stress grows to an adequately high level, the asperities are severely damaged. That is to say, the shear behaviour of the rock joint is controlled by asperity degradation. Dilation and degradation of asperities occur concurrently for a rock joint subjected to shear under non-extreme normal stress conditions. Several models have been proposed to quantify the degradation of joint asperities, most of which suffer the following limitations. First, the applicability of the models is limited to two-dimensional joints with idealised profiles (Ladanyi and Archambault 1969; Plesha 1987; Saeb and Amadei 1992). Second, the models are highly empirical, lacking solid theoretical foundation (Barton and Choubey 1977; Grasselli and Egger 2003; Asadollahi and Tonon 2010; Li et al. 2018). Third, the models commonly demand more than one coefficients, the determination of which relies on back-analysing experimental data or empirical judgement (Schneider 1976; Lee et al. 2001; Ghazvinian et al. 2012; Oh et al. 2015). Thus, the practicality of these models in the field is still under examination. Fourth, few models have considered the roles of waviness and unevenness playing in shear. The dilation and degradation of waviness and

unevenness mutually dictate the shear stress evolution as shear proceeds (Li et al. 2016, 2017, 2018).

This paper presents an analytical model for the shear behaviour of rock joints with two-order asperities. Waviness and unevenness are separated through wavelet analysis, based on which critical waviness and critical unevenness are quantitatively determined. The dilation and degradation of critical waviness and critical unevenness are, respectively, predicted by considering the dominance of plastic tangential work in asperity deterioration. The sheared areas of two-order asperities are assessed by accounting for the true asperity areas participating in shear. The capability of the analytical model is illustrated by correlating with experimental data from both sawtooth- and natural-shaped joints.

## 2 Analytical Modelling

### 2.1 Problem Description

We consider a rock block cut by a tightly closed joint (Fig. 1). The upper block under a normal stress ( $\sigma_n$ ) can move vertically, and the lower part is restricted to displace horizontally subjected to a shear stress ( $\tau$ ). The joint asperities consist of waviness and unevenness. The mechanical contributions of waviness and unevenness to shear resistance can be separately represented by critical waviness and critical unevenness (Li et al. 2016). Geometrical properties of the two-order asperities include the initial inclination angles ( $i_0$  and  $\alpha_0$ ), wavelength ( $\lambda_w^0$  and  $\lambda_u^0$ ), and amplitude ( $A_w^0$  and  $A_u^0$ ) of critical waviness and critical unevenness, respectively. In the following, we show the determination of critical waviness and critical unevenness of a natural joint profile.

### 2.2 Roughness Decomposition

Waviness and unevenness of a rock joint occur in varying scales. Waviness initially refers to large-scale undulations in the field, and unevenness represents small-scale asperities that are observed in the laboratory (Patton 1966; ISRM 1978). The roughness of a laboratory-scale joint also comprises waviness and unevenness (Jing et al. 1992; Yang et al. 2001; Lee et al. 2001). Waviness with comparatively larger wavelength mainly contributes to the dilation behaviour, whereas unevenness of a smaller asperity size is sheared off and broken, providing shear resistance to the shear movement. The roles of waviness and unevenness playing in shear can be correspondingly represented by a critical waviness and a critical unevenness (Li et al. 2016, 2017). The critical waviness was practically determined as the waviness with the highest amplitude along the shear direction, and the critical unevenness is the unevenness with the longest wavelength on the critical waviness (Li et al. 2016, 2017).

This pragmatic approach is effective for a joint profile with unmissable undulations and unevenness, whereas natural joints, particularly those with low degree roughness, may exhibit waviness and unevenness that are hardly discernable. Therefore, a quantitative approach is required to decompose joint roughness into waviness and unevenness at different scales. Recently, wavelet analysis stemming from signal processing has been utilised to isolate waviness from unevenness, for the purpose of studying joint permeability (Zou et al. 2015), implying the potential of the method for predicting the shear behaviour of rock joints with waviness and unevenness.

Following the approach of Zou et al. (2015), Fig. 2 illustrates the decomposition of a natural joint profile into waviness and unevenness through wavelet analysis. The Wavelet Design and Analysis Toolbox in Matlab is utilised to perform the analysis. A digitised joint profile is imported into the toolbox. The Daubechies' wavelet (db8) producing the best match of the joint profile is used as the mother wavelet. The fourth level of the approximation profile is determined as waviness. Unevenness is acquired by subtracting waviness from the original profile. To remove the noise of unevenness, wavelet analysis is conducted again. Critical waviness is easily determined as the undulation with largest wavelength and amplitude along shear direction. The critical unevenness is chosen as the largest asperity on the critical waviness (Fig. 2b). The geometrical properties of critical waviness and critical unevenness are measured.

### 2.3 Model Framework

Li et al. (2016, 2017, 2018) reported that the shear behaviour of a rock joint is governed by the mobilisation of waviness and unevenness. For a rock joint under shear, there is a bounding or mobilisable shear strength ( $\tau_m$ ) that represents the maximum reachable shear stress, resembling the continuously-yielding model (Cundall and Hart 1984). Figure 3 shows typical shear stress–shear displacement and dilation–shear displacement relationships based on the mobilisable shear strength model.

The mobilisable shear strength of a natural rock joint ( $\tau_m$ ) consists of strength components to overcome basic friction, dilation, and degradation of critical waviness and critical unevenness, respectively:

$$\tau_m = \sigma_n \tan(\phi_b + i_d^m + \alpha_d^m)(1 - a_s) + a_s \sigma_T^s, \quad (1)$$

where  $i_d^m$  and  $\alpha_d^m$  represent the mobilisable dilation angles of critical waviness and critical unevenness, respectively. The mobilisable dilation angle is contributed by critical waviness and critical unevenness is

$$\alpha_n^m = i_d^m + \alpha_d^m. \quad (2)$$

$a_s$  denotes the sheared area ratio, which equals

$$a_s = \frac{S_w^s + S_u^s}{S_w^0 + S_u^0}, \quad (3)$$

where  $S_w^s$  and  $S_u^s$  denote the sheared areas of critical waviness and critical unevenness, respectively, and  $S_w^0$  and  $S_u^0$  represent the initial areas of critical waviness and critical unevenness, correspondingly.

$\sigma_T^s$  in Eq. (1) is the transitional shear stress, subjected to which the asperities are completely sheared off without joint dilation, and is estimated as:

$$\sigma_T^s = \sigma_T^n \tan \phi_b, \quad (4)$$

where  $\phi_b$  is the joint basic friction angle, and  $\sigma_T^n$  is the transitional normal stress (Ladanyi and Archambault 1969; Gerard 1986; Saeb and Amadei 1992; Li et al. 2018).

The shear stress–shear displacement and dilation–shear displacement curves of a rock joint under shear can be predicted based on the mobilisable shear strength. Upon shear loading, joint asperities deform elastically, producing a linear relationship between shear stress increment ( $d\tau$ ) and shear displacement increment ( $d\delta_s^e$ ), that is

$$d\tau = k_s d\delta_s^e, \quad (5)$$

where  $k_s$  denotes the joint shear stiffness.

In the elastic stage, the joint dilation angle ( $d_n$ ) is zero, whereas the mobilisable dilation angle ( $d_n^m$ ) decreases from the maximum value which equals the sum of the initial inclination angles of the critical waviness and the critical unevenness ( $i_0 + \alpha_0$ ) (Fig. 2). Once the shear stress exceeds the basic frictional strength ( $\tau_b = \sigma_n \tan \phi_b$ ) (Oh et al. 2015), the joint enters the plastic stage due to asperity degradation, where dilation commences. The mobilisable dilation angle ( $d_n^m$ ) continues to decrease. The dilation angle ( $d_n$ ) is maximum at the beginning of plastic stage, followed by continuous decrease as shear proceeds. During the whole shear process, the mobilisable shear strength  $\tau_m$  reduces due to the deformation of waviness and unevenness. The shear stress ( $\tau$ ) in the plastic stage is dictated by the shear stiffness that is the slope of the shear stress–shear displacement curve ( $Fk_s$ ), where  $F$  is a reduction factor and depends on the difference between the shear stress ( $\tau$ ) and the mobilisable shear strength ( $\tau_m$ ) (Cundall and Hart 1984), that is

$$F = 1 - \frac{\tau}{\tau_m}. \quad (6)$$

When the critical waviness and the critical unevenness are entirely sheared off at a sufficiently large shear displacement, the shear stress ( $\tau$ ) equals the mobilisable shear strength ( $\tau_m$ ) (Fig. 2).

### 2.4 Asperity Degradation

In the plastic stage, asperities are degraded and dilation occurs, resulting in the shear stress variation. The degradation of an asperity depends on the combination of shear stress and shear displacement (Plesha 1987). Based on the classic wear theory (Queener et al. 1965; Leong and Randolph 1992; Li et al. 2016) and considering plastic tangential work, for the critical waviness, we propose that the increment of the sheared area of the critical waviness ( $dS_w^s$ ) over the increment of plastic tangential work ( $dW_s^p$ ) is linearly proportionate with the unsheared area of the critical waviness ( $S_w$ ), that is

$$\frac{dS_w^s}{dW_s^p} = c_w S_w, \tag{7}$$

where the increment of plastic tangential work ( $dW_s^p$ ) is the product of shear stress and plastic shear displacement increment, i.e.,  $dW_s^p = \tau d\delta_s^p$ .  $c_w$  is the degradation coefficient of the critical waviness with a unit of length / force.

Considering the area variation of the unsheared area of the critical waviness ( $S_w$ ) due to plastic shear displacement, as illustrated in Fig. 4, the unsheared area of the critical waviness ( $S_w$ ) is

$$S_w = \frac{A_w \lambda_w}{2} = \frac{(\lambda_w^0 - 2\delta_s^p)^2}{2(\cot i_d + \cot i_0)} \tag{8}$$

**Table 1** Input parameters used in the analytical model for predicting the shear behaviours of sawtooth-shaped joints with 20° and 30° initial inclination angles

Critical waviness			$\sigma_n$ (MPa)	$k_s$ (MPa/mm)	$\delta_{ms}^e$ (mm)	$K$
$i_0$ (°)	$\lambda_w^0$ (mm)	$A_w^0$ (mm)				
20	25	4.55	1.5	1.56	1.10	0.6
			3.5	2.76	1.67	
			5.0	2.98	2.35	
30	25	7.22	1.0	1.94	1.36	
			3.0	2.60	2.16	
			5.0	3.28	2.37	

Note that the sinusoidal-shaped critical waviness is simplified triangular.

The sheared area of the critical waviness is

$$S_w^s = S_w^0 - S_w - S_w^b, \tag{9}$$

where  $S_w^b$  is the area of the critical waviness base that is no longer involved in shear due to dilation, and is calculated as

$$S_w^b = \int_0^{\delta_n} \frac{(\lambda_w + \lambda_w^0 - 2\delta_s^p)}{2} d\delta_n. \tag{10}$$

Combining Eqs. (7) and (8), the sheared and unsheared areas of the critical waviness are, respectively

$$S_w^s = (S_w^0 - S_w^b)(1 - e^{-c_w W_s^p}) \tag{11a}$$

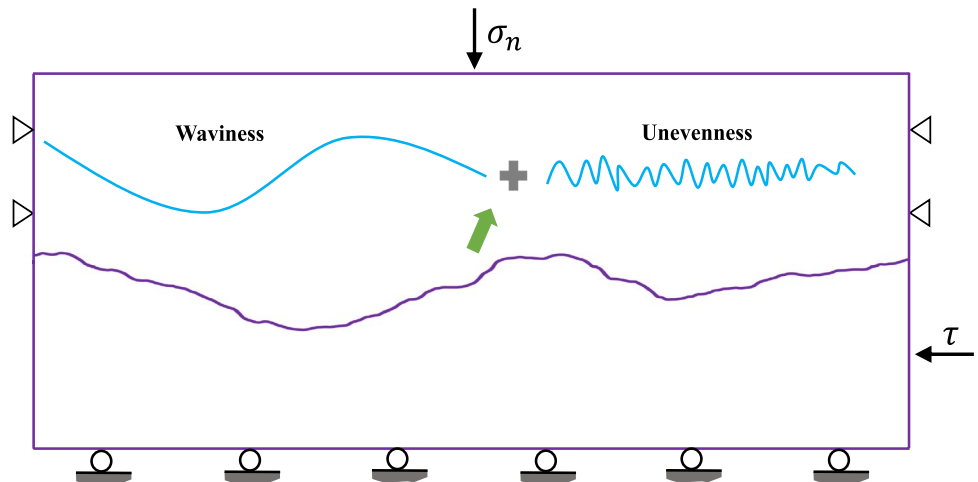
$$S_w = (S_w^0 - S_w^b) e^{-c_w W_s^p}. \tag{11b}$$

Thus, the sheared area of the critical waviness is

$$S_w^s = S_w^0 - S_w - S_w^b = \frac{\lambda_w^0 A_w^0}{2} - \frac{(\lambda_w^0 - 2\delta_s^p)^2}{2(\cot i_d + \cot i_0)} - S_w^b. \tag{12}$$

Equating Eqs. (11b) and (8) yields the dilation angle of the critical waviness ( $\tan i_d$ ):

**Fig. 1** Illustration of a natural rock joint subjected to shear ( $\tau$ ) under a normal stress ( $\sigma_n$ )



$$\tan i_d = \frac{2 \tan i_0 (S_w^0 - S_w^b) e^{-c_w W_s^p}}{\tan i_0 (\lambda_w^0 - 2\delta_s^p)^2 - 2(S_w^0 - S_w^b)} \quad (13)$$

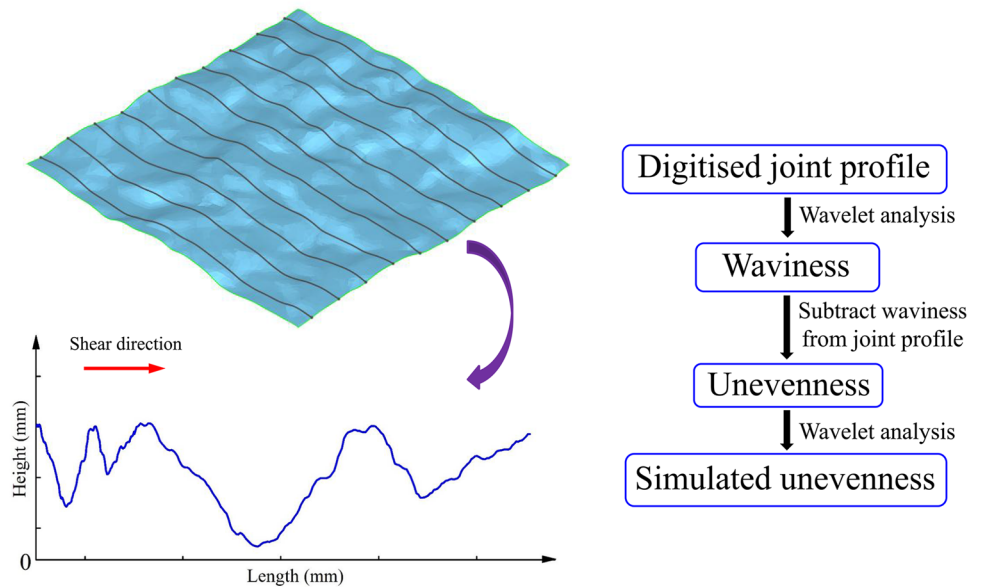
The sheared area ratio of the critical waviness ( $a_w^s$ ) is

$$a_w^s = \frac{S_w^s}{S_w^0} \quad (14)$$

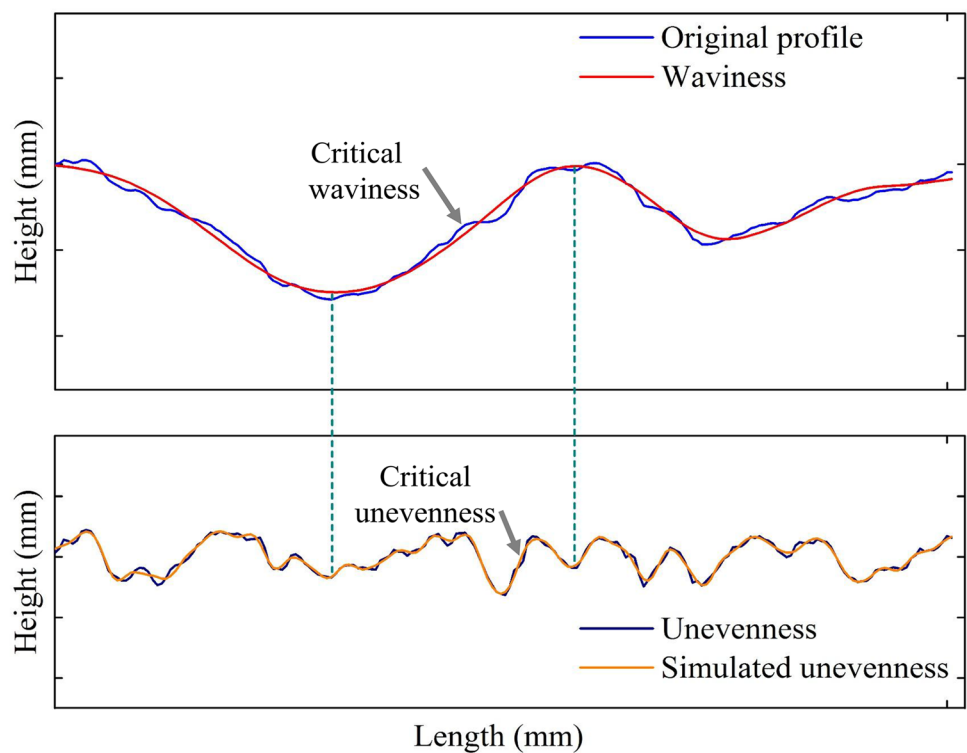
The mobilisable dilation angle of the critical waviness in the elastic stage decreases as the elastic tangential energy ( $W_s^e = \int \tau d\delta_s^e$ ) accumulates in the asperity:

$$\tan i_d^m = \frac{e^{-c_w W_s^e}}{2 - e^{-c_w W_s^e}} \tan i_0 \quad (15)$$

**Fig. 2** Roughness decomposition using wavelet analysis



**(a)** Procedures of wavelet analysis for a digitised joint profile



**(b)** Determination of waviness and unevenness through wavelet analysis

**Table 2** Input parameters used in the analytical model for predicting the shear behaviour of the JRC-shaped joints

Sample	$\sigma_n$ (MPa)	Critical waviness			Critical unevenness			$k_s$ (MPa/mm)	$\delta_{ms}^e$ (mm)	$K$
		$i_0$ (°)	$\lambda_w^0$ (mm)	$A_w^0$ (mm)	$\alpha_0$ (°)	$\lambda_u^0$ (mm)	$A_u^0$ (mm)			
JRC 4–6	1	1.7	60	0.9	5.1	16	0.71	0.67	0.5	0.5
JRC 10–12	3.5	9.3	60	4.9	7.2	10	0.63	1.5	1.0	
JRC 14–16	5.0	12.4	53	5.8	12.7	8.0	0.9	2.7	1.3	

**Table 3** Input parameters used in the analytical model for predicting the shear behaviour of the irregular joints in Flamand et al. (1994)

Critical waviness			Critical unevenness			Elastic stage	$\sigma_n$ (MPa)			$K$
$i_0$ (°)	$\lambda_w^0$ (mm)	$A_w^0$ (mm)	$\alpha_0$ (°)	$\lambda_u^0$ (mm)	$A_u^0$ (mm)		7	14	21	
5.1	35.2	1.6	14.0	4.0	0.5	$k_s$ (MPa/mm)	32.7	53.5	62.8	0.2
						$\delta_{ms}^e$ (mm)	0.34	0.25	0.28	

The degradation coefficient of the critical waviness ( $c_w$ ) relies on the geometric properties of the asperity and the uniaxial compressive strength of the rock ( $\sigma_c$ ):

$$c_w = K \frac{i_d}{\sigma_c \sqrt{S_w}}, \tag{16}$$

where  $K$  is a dimensionless constant that represents the influence of experimental environments, such as humidity and temperature, on the degradation process of waviness.

Similarly, for the critical unevenness, the mobilisable dilation angle of the critical unevenness in the elastic stage ( $\tan \alpha_d^m$ ) is

$$\tan \alpha_d^m = \frac{e^{-c_u W_s^e}}{2 - e^{-c_u W_s^e}} \tan \alpha_0, \tag{17}$$

where  $\alpha_0$  denotes the initial inclination angle of the critical unevenness, and  $c_u$  is the degradation coefficient of the critical unevenness.

In the plastic stage, we have

$$\tan \alpha_d = \frac{2 \tan \alpha_0 (S_u^0 - S_u^b) e^{-c_u W_s^p}}{\tan \alpha_0 (\lambda_u^0 - 2\delta_s^p)^2 - 2(S_u^0 - S_u^b)} \tag{18a}$$

$$S_u^s = \frac{\lambda_u^0 A_u^0}{2} - \frac{(\lambda_u^0 - 2\delta_s^p)^2}{2(\cot \alpha_d + \cot \alpha_0)} - S_u^b \tag{18b}$$

$$S_u^b = \int_0^{\delta_n} \frac{(\lambda_u + \lambda_u^0 - 2\delta_s^p)}{2} d\delta_n \tag{18c}$$

$$a_u^s = \frac{S_u^s}{S_u^0} \tag{18d}$$

**Table 4** Average percent errors ( $\delta_{ave}$ ) between experimental data and analytical predictions

Experiments	Cases	$\delta_{ave}(\tau)$ (%)	$\delta_{ave}(\delta_n)$ (%)
20°	$\sigma_n = 1.5$ MPa	5.2	6.1
	$\sigma_n = 3.5$ MPa	8.7	5.3
	$\sigma_n = 5.0$ MPa	8.5	6.4
30°	$\sigma_n = 1.0$ MPa	11.4	11.5
	$\sigma_n = 3.0$ MPa	10.7	12.3
	$\sigma_n = 5.0$ MPa	6.3	10.2
JRC 4-6	$\sigma_n = 1.0$ MPa	8.5	8.3
JRC 10-12	$\sigma_n = 3.5$ MPa	7.9	17.4
JRC 14-16	$\sigma_n = 5.0$ MPa	10.7	15.4
Flamand et al. (1994)	$\sigma_n = 7.0$ MPa	5.2	11.1
	$\sigma_n = 14.0$ MPa	9.1	10.9
	$\sigma_n = 21.0$ MPa	8.5	10.7

$$c_u = K \frac{\alpha_d}{\sigma_c \sqrt{S_u}}, \tag{18e}$$

where  $A_u^0$ ,  $\lambda_u^0$ , and  $S_u^0$  are the initial amplitude, wavelength, and area of the critical unevenness, respectively.  $\alpha_d$  and  $\lambda_u$  denote the dilation angle and wavelength of the critical unevenness under shearing, respectively.  $S_u$  and  $S_u^s$  are the unsheared and sheared areas of the critical unevenness, respectively.  $S_u^b$  is the area of the critical unevenness base, and  $a_u^s$  is the sheared area ratio of the critical unevenness.

### 3 Model Validation

#### 3.1 Model Implementation

Figure 5 illustrates the procedures for implementing the proposed model. Equation (5) yields the linear relationship

between the shear stress and the shear displacement in the elastic stage. Once the shear displacement exceeds the maximum elastic shear displacement ( $\delta_{ms}^e$ ), plastic deformation appears accompanied by asperity degradation. Equation (6) is employed to continuously update the shear stiffness, i.e., the slope of the shear stress–shear displacement curve. When the shear displacement reaches the prescribed value, i.e., the iterative step ( $i$ ) equals the maximum loop number ( $n$ ), the calculation ends and outputs shear stress, dilation, and shear displacement.

The model’s validity has been demonstrated by comparing with the experimental data from direct shear tests on

both sawtooth- and irregular-shaped joints under varying normal stresses. The shear stiffness ( $k_s$ ) and the maximum shear displacement ( $\delta_{ms}^e$ ) are obtained based on the experimental curves. The transitional normal stress is conveniently assessed as 20%–30% of the uniaxial compressive strength of the rock (Flamand 2000; Grasselli and Egger 2003).

### 3.2 Model Validation

We performed direct shear tests on both sawtooth- and JRC-shaped joints with a Geotechnical Consulting and Testing Systems (GCTS) servo-hydraulic testing machine, RDS-300

**Fig. 3** Shear stress–shear displacement and dilation–shear displacement relationships based on the mobilisable shear strength model.  $\tau$ ,  $\tau_b$ , and  $\tau_m$  denote shear stress, basic frictional strength, and mobilisable shear strength, respectively.  $\delta_{ms}^e$ ,  $\delta_s$ , and  $\delta_n$  represent maximum elastic shear displacement, shear displacement, and dilation, correspondingly.  $d_n$  and  $d_n^m$  are dilation angle and mobilisable dilation angle, respectively.  $i_0$  and  $\alpha_0$  refer to inclination angles of the critical waviness and the critical unevenness, separately.  $k_s$  denotes joint shear stiffness, and  $F$  is the reduction factor.  $d\tau$ ,  $d\delta_n$ , and  $d\delta_s$  are increments of shear stress, dilation, and shear displacement, respectively

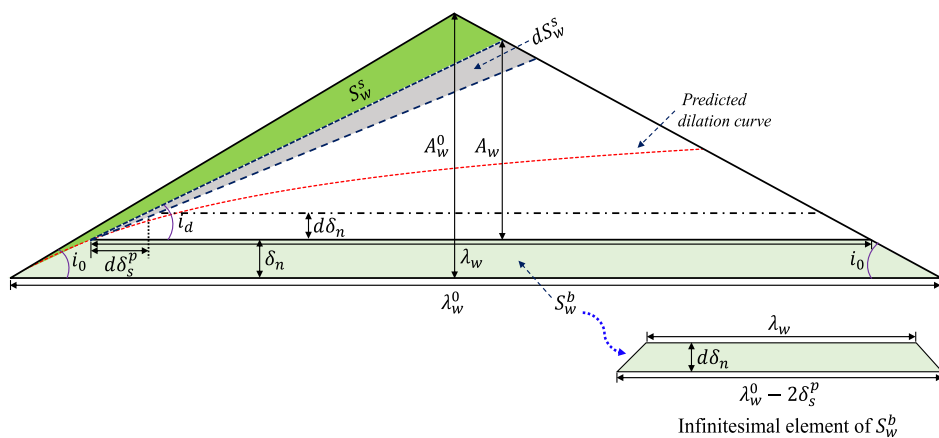
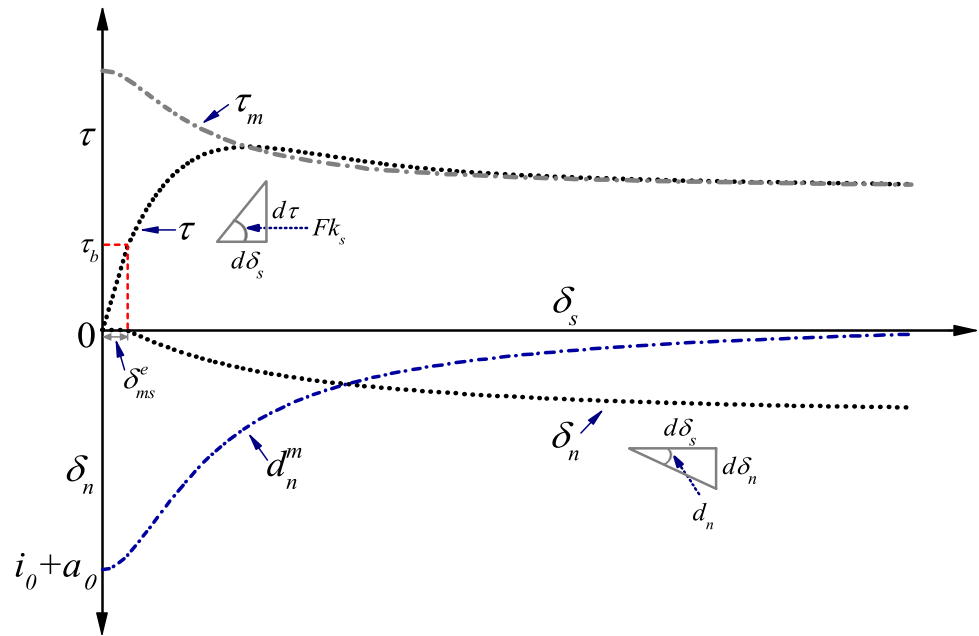
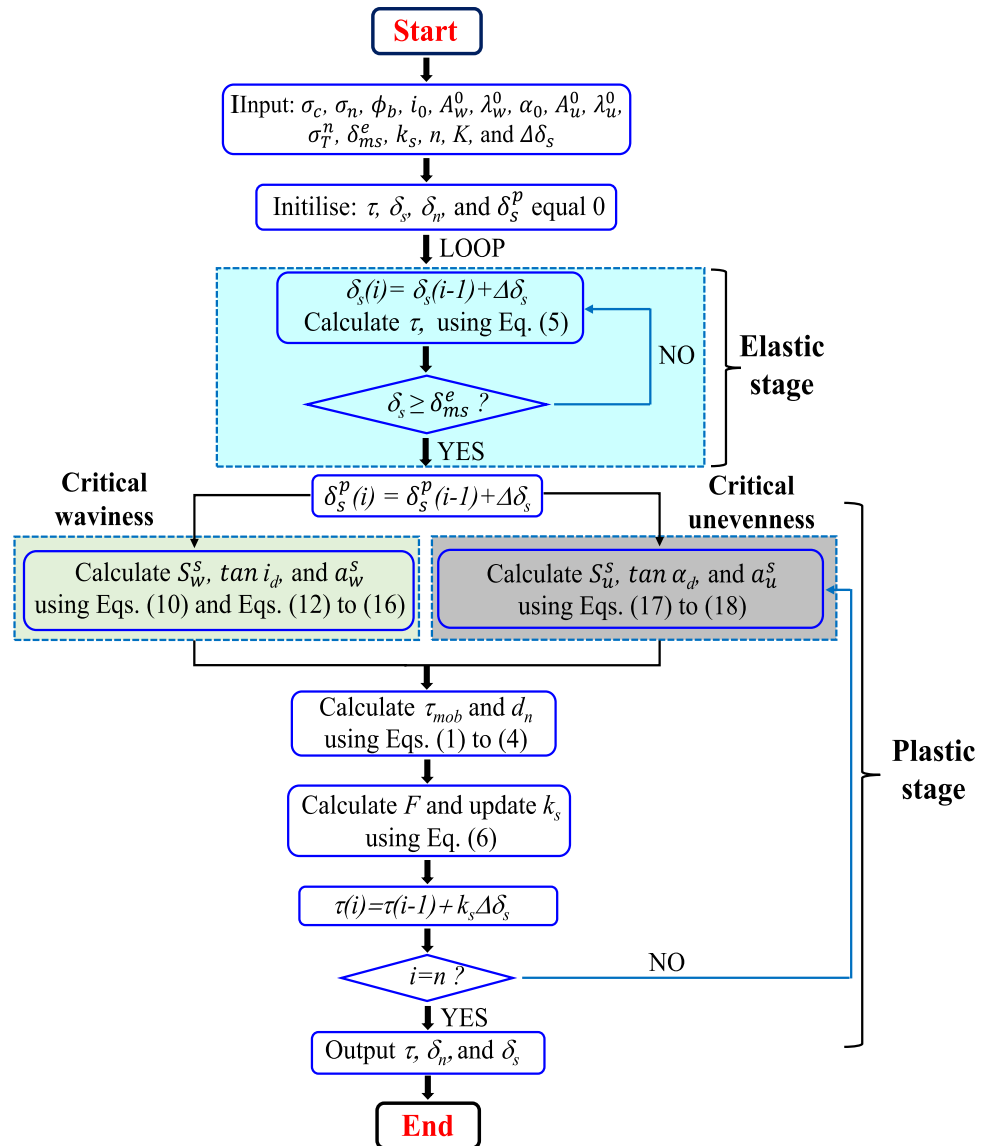


**Fig. 4** Degradation process of a sawtooth-shaped critical waviness.  $i_0$ ,  $\lambda_w^0$ , and  $A_w^0$  are the initial inclination angle, wavelength, and amplitude of the critical waviness, respectively.  $i_d$ ,  $\lambda_w$ , and  $A_w$  are the dilation angle, wavelength, and amplitude of the critical waviness under shearing.  $d\delta_s^p$  and  $d\delta_n$  are the incremental plastic shear displacement

and the incremental dilation, respectively.  $\delta_n$  denotes dilation.  $S_w^s$  is the sheared area of the critical waviness, and  $dS_w^s$  is the incremental sheared area of the critical waviness.  $S_w^b$  is the area of the critical waviness base

**Fig. 5** Flowchart for model implementation



(Li 2016). Two types of sawtooth-shaped joints with the same wavelength of 25 mm and different initial inclination angles of triangular asperities, i.e., 20° and 30°, and three types of JRC-shaped joints, i.e., JRC 4–6, JRC 10–12, and JRC 14–16, were prepared (Fig. 6). The digitising interval of the standard JRC profiles was 0.5 mm. To ensure that the profiles of the replicas were as identical as possible, cast moulds were designed and manufactured of high-strength stainless steel. Figure 7a–c illustrates the decomposition of the three JRC profiles, respectively.

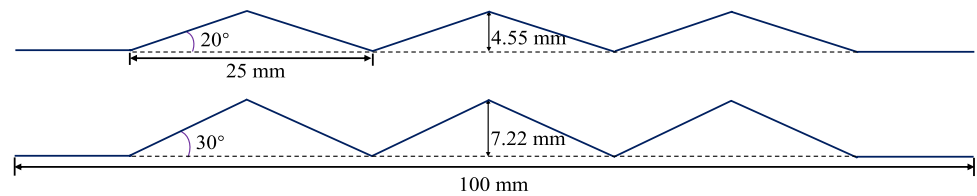
The synthetic joints were made of the Hydrostone gypsum cement, which consisted of  $\text{CaSO}_4 \cdot \text{H}_2\text{O} > 95\%$  and Portland cement  $< 5\%$ . The cement and water were mixed at a weight ratio of 1:0.35. All the samples dimensioned 100 mm  $\times$  100 mm  $\times$  100 mm were seasoned at 42°C in a curing oven for 14 days. The uniaxial compressive strength

of the cement mixture was 46.3 MPa, the tensile strength was 2.4 MPa, and the basic friction angle was 42°. The transitional normal stress was estimated at  $0.2 \sigma_c$ .

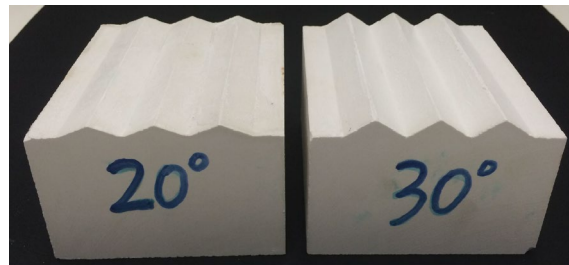
We analytically simulated the shear stress and dilatancy of the sawtooth- and JRC-shaped joints under different normal stresses from 1.0 to 5.0 MPa. Tables 1 and 2 detail the input parameters used in the analytical model. Figures 8, 9 and 10 show an overall good agreement between the analytical predictions and the experimental data. Some differences appear between the analytical and the experimental curves in the post-peak stages, particularly for the sawtooth-shaped joints under higher normal stresses (Figs. 8, 9). These discrepancies mainly resulted from the brittle dynamic failure of the regular asperities, which are not well captured by the proposed model that assumes asperities undergo gradual degradation. For the JRC-shaped joints, the predicted



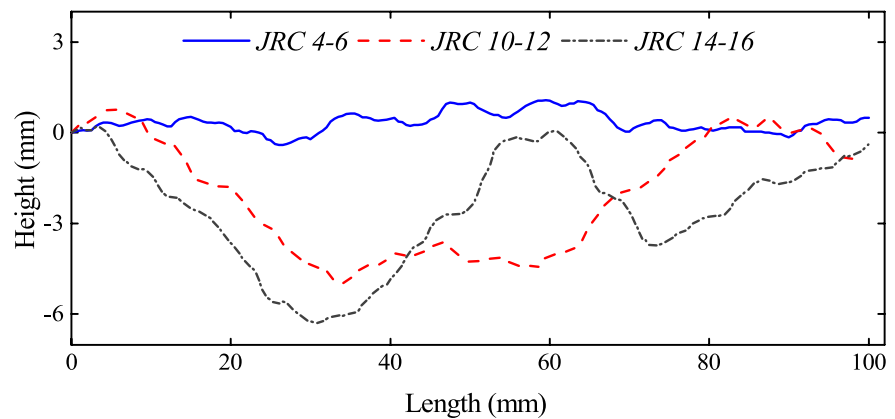
**Fig. 6** Sawtooth- and JRC-shaped joint samples used in the direct shear tests



(a) Sawtooth-shaped joint profiles.



(b) Hydrostone joints used in the direct shear tests.



(c) Digitised standard joint profiles of *JRC 4-6*, *JRC 10-12*, and *JRC 14-16*



(d) Joint samples with *JRC*-shaped profiles

dilatancy does not match the experimentally observed values very well (Fig. 10). The omission of higher order (third or fourth) asperities is mainly responsible for the disagreement, as higher order asperities have more pronounced influence on dilation than shear stress.

We further compared the analytical predictions to the experimental data of joints with natural profiles. Flamand et al. (1994) carried out direct shear tests on synthetic joints

cast from the natural joints sourced in the Guèret granite (France). Figure 7d shows the decomposition of the joint profile. The non-shrinking mortar was used to replicate joint samples with a diameter of 90 mm. The uniaxial compressive strength of the mortar was 82 MPa, the tensile strength was 6.6 MPa, and the basic friction angle was 37°. The transitional normal stress was estimated at  $0.3 \sigma_c$ .

We analytically reproduced the shear stress–shear displacement and dilation–shear displacement curves of the irregular-shaped joints under three different normal stresses, namely, 7 MPa, 14 MPa, and 21 MPa. Table 3 lists the input parameters used in the analytical prediction.

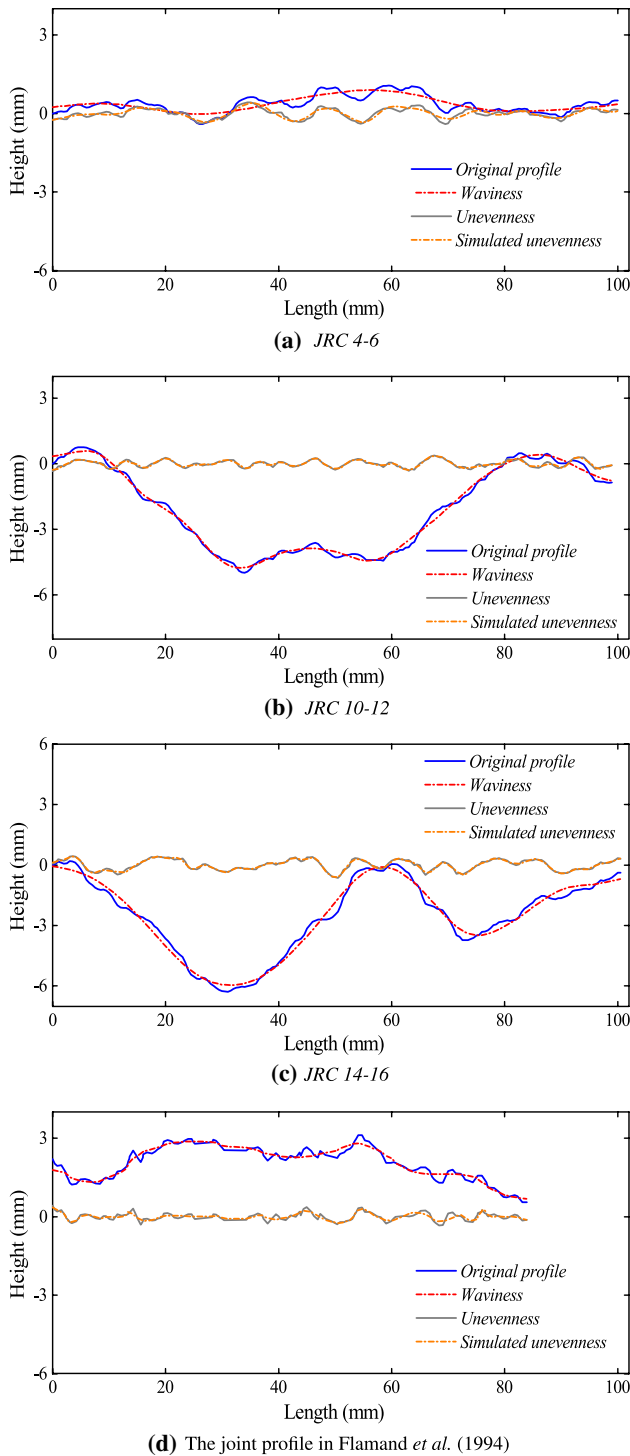


**Fig. 7** Roughness decomposition of three JRC profiles and the joint profile in Flamand et al. (1994)

Figure 11 shows that the proposed model predicts effectively the shear stress–shear displacement behaviour, but slightly overestimates the dilation–shear displacement relationship. This overestimation of dilation possibly results from the fact that one two-dimensional joint profile may be inadequate to describe the joint surface characteristics reproduced from natural joints.

We demonstrated the performance of the proposed model by comparing the analytical predictions to the experimental data obtained from direct shear tests on sawtooth- and irregular-shaped joints under different normal stresses. To quantify the accuracy of the analytical predictions, the average percent error ( $\delta_{ave}$ ) is used as a precision indicator. The average percent errors of shear stress ( $\delta_{ave}(\tau)$ ) and dilation ( $\delta_{ave}(\delta_n)$ ) are, respectively:

$$\delta_{ave}(\tau) = \frac{1}{z} \sum_{m=1}^z \left| \frac{\tau^{\text{exp}} - \tau^{\text{pre}}}{\tau^{\text{pre}}} \right| \times 100\% \quad (19a)$$

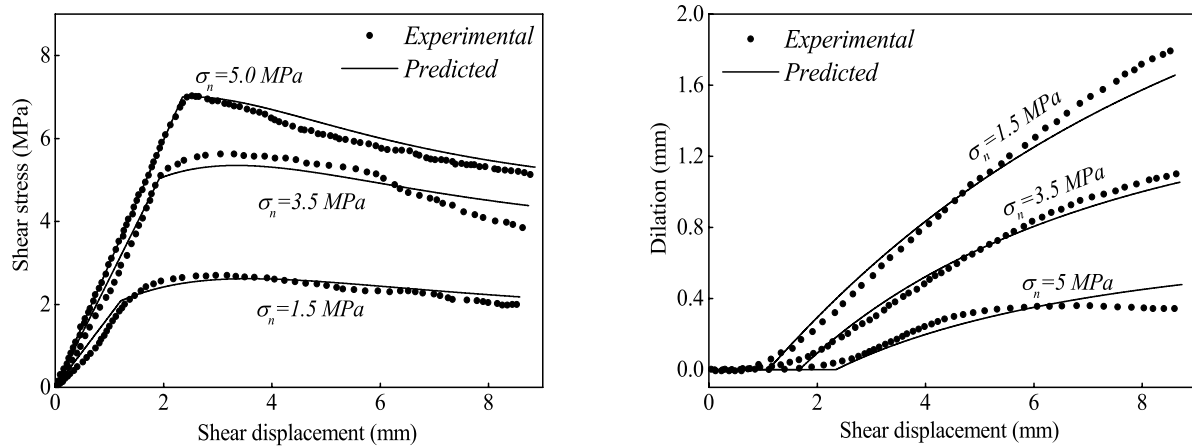
$$\delta_{ave}(\delta_n) = \frac{1}{z} \sum_{m=1}^z \left| \frac{\delta_n^{\text{exp}} - \delta_n^{\text{pre}}}{\delta_n^{\text{exp}}} \right| \times 100\%, \quad (19b)$$

where  $z$  is the number of data for analysis,  $\tau^{\text{exp}}$  and  $\tau^{\text{pre}}$  denote the experimental and the analytical shear stresses, respectively;  $\delta_n^{\text{exp}}$  and  $\delta_n^{\text{pre}}$  are the experimental and the predicted dilation, separately.

Table 4 lists the average percent errors of shear stress and dilation between the experimental data and the analytical predictions. For all cases, the average percent errors are lower than 18%, most of which do not exceed 15%. Therefore, the proposed model satisfactorily predicts the shear behaviour of rock joints under direct shear. However, the capability of the proposed model can be further improved by incorporating the sudden brittle breakage of large asperities in the post-peak stage and the effect of higher order asperities on the shear behaviour of rock joints.

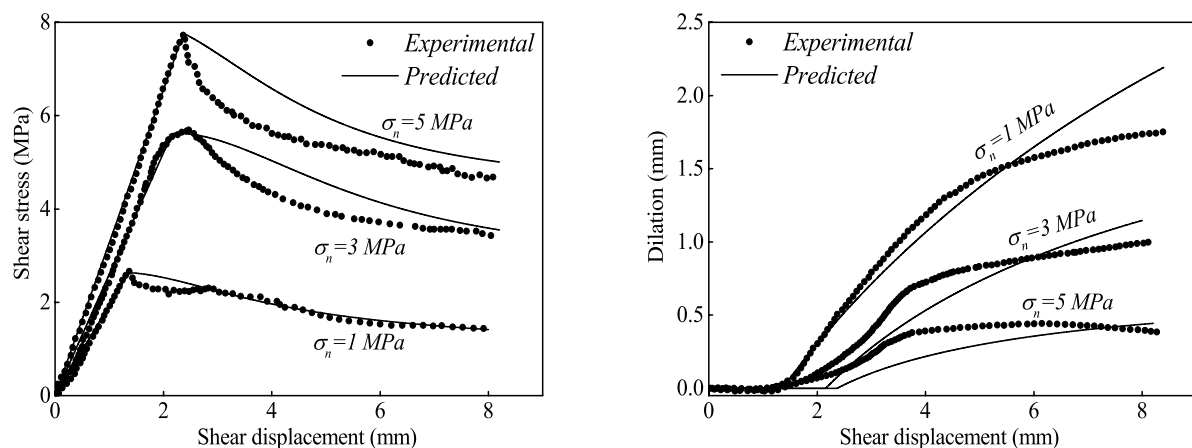
## 4 Discussion

In this paper, the shear behaviour of a rock joint exhibiting two-order roughness is analytically modelled. The proposed model possesses the following advantages. First, critical waviness and critical unevenness are determined based on quantifiable separation of waviness and unevenness through wavelet analysis technique. Second, asperity degradation is predicted by establishing the relationship between asperity area variation and plastic tangential work, which mimics the physically motivated process of asperity evolution. Third, the model reproduces the non-linear variations of shear stress and dilation of a rock joint under shearing with



**(a)** Shear stress-shear displacement curves under normal stresses of 1.5 MPa, 3.5 MPa, and 5 MPa, respectively **(b)** Dilation-shear displacement curves under normal stresses of 1.5 MPa, 3.5 MPa, and 5 MPa, respectively

**Fig. 8** Comparison between the analytical predictions and the experimental curves from direct shear tests on the sawtooth-shaped joints with 20° initial inclination angle



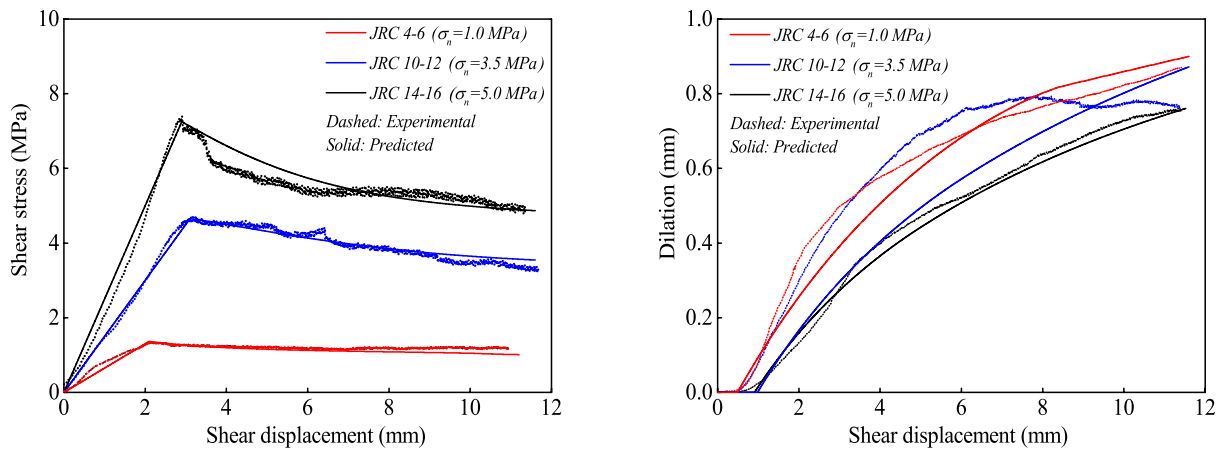
**(a)** Shear stress-shear displacement curves under normal stresses of 1 MPa, 3 MPa, and 5 MPa, respectively **(b)** Dilation-shear displacement curves under normal stresses of 1 MPa, 3 MPa, and 5 MPa, respectively

**Fig. 9** Comparison between the analytical predictions and the experimental curves from direct shear tests on the sawtooth-shaped joints with 30° initial inclination angle

acceptable accuracy, as demonstrated by the comparison between analytical predictions and experimental data.

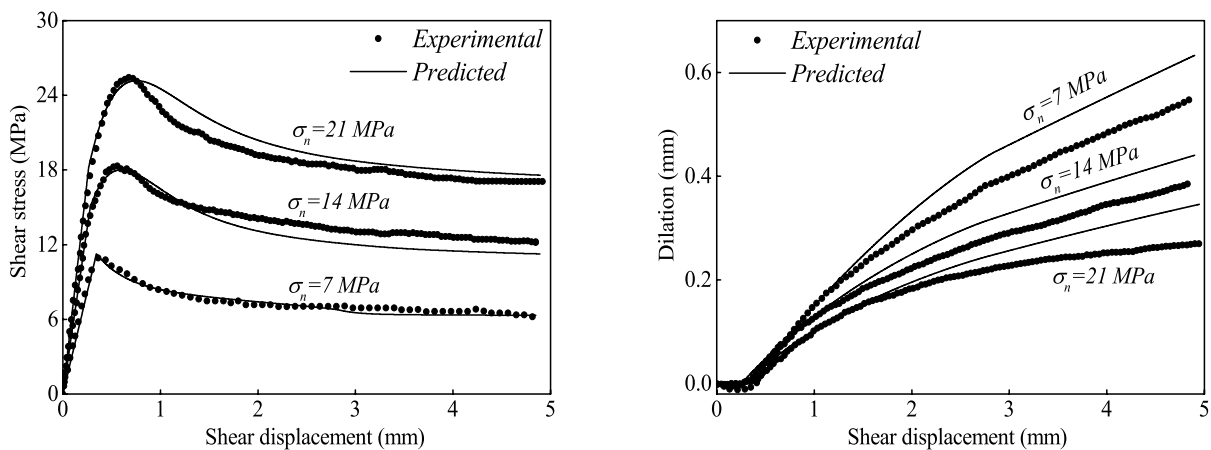
Although the proposed model owns the above-mentioned strengths, it has limitations. First, transitional normal stress is empirically determined as 20–30%  $\sigma_c$  based on limited experimental data of Flamand (2000) and Grasselli and Egger (2003). The magnitude of transitional normal stress depends on a number of variables such as rock mineralogy, joint roughness, and porosity (Wong and Baud 2012).

Accurate acquisition of transitional normal stress requires performing direct shear tests in the high normal stress range. Second, the dimensionless coefficient  $K$  in Eqs. (16) and (17) was obtained by back-analysing experimental data. The estimation of  $K$  is quite challenging based on our current understanding on asperity degradation, since it depends heavily on the experimental environments such as humidity and temperature.



**(a)** Shear stress-shear displacement curves of three *JRC*-shaped joints under normal stresses of 1.0 MPa, 3.5 MPa, and 5.0 MPa, respectively **(b)** Dilation-shear displacement curves of three *JRC*-shaped joints under normal stresses of 1.0 MPa, 3.5 MPa, and 5.0 MPa, respectively

**Fig. 10** Comparison between the analytical predictions and the experimental curves from direct shear tests on three *JRC*-shaped joints



**(a)** Shear stress-shear displacement curves under normal stresses of 7 MPa, 14 MPa, and 21 MPa, respectively **(b)** Dilation-shear displacement curves under normal stresses of 7 MPa, 14 MPa, and 21 MPa, respectively

**Fig. 11** Comparison between the analytical predictions and the experimental curves from direct shear tests on the irregular joints in Flamand et al. (1994)

## 5 Conclusions

This paper introduces an analytical model for the mechanical behaviour of a rock joint subjected to shear. Two-order asperities, i.e., waviness and unevenness of a natural joint profile, were separated using wavelet analysis method. Critical waviness and critical unevenness were, respectively, chosen to represent the mechanical involvements of waviness and unevenness in shear. The evolution of each-order asperity was quantified by formulating the

relationships among plastic tangential work, sheared and unshaded asperity areas. The dilation angle of each-order asperity decreased over the accumulation of plastic tangential work. The incremental sheared asperity area was assessed by considering the asperity area truly involved in shear. The proposed model was validated against experimental results from direct shear tests on sawtoothed, *JRC*-shaped, and natural-profiled joints. The analytical predictions overall matched the experimental curves, although some discrepancies appeared. The performance of the

proposed model can be improved by accounting for the effect of higher order asperities on joint shear behaviour. The developed model, after being implemented in finite and discrete element codes, is practicable to appraise the stability of rock-engineering structures.

**Acknowledgements** Yingchun Li thanks the financial supports from the National Natural Science Foundation (Grant No. 51809033), the China Postdoctoral Science Foundation (Grant No. 2018M631789), the National Key Research and Development Plan (Grant No. 2018YFC1505301), and the Fundamental Research Funds for the Central Universities (Grant No. DUT17RC(3)032).

## References

- Asadollahi P, Tonon F (2010) Constitutive model for rock fractures: revisiting Barton's empirical model. *Eng Geol* 113(1):11–32
- Barton N (1973) Review of a new shear-strength criterion for rock joints. *Eng Geol* 7(4):287–332
- Barton N, Choubey V (1977) The shear strength of rock joints in theory and practice. *Rock Mech* 10(1–2):1–54
- Cundall P, Hart R (1984) Analysis of block test No. 1 inelastic rock mass behavior: phase 2-A characterization of joint behavior (final report). Technical report, Itasca Consulting Group, Inc., Minneapolis, Minnesota (USA)
- Flamand R (2000) Validation of a model of mechanical behavior for rock fractures in shear. Ph.D. thesis, University of Quebec, Chicoutimi (*in French*)
- Flamand R, Archambault G, Gentier S, Riss J, Rouleau A (1994) An experimental study of the shear behavior of irregular joints based on angularities and progressive degradation of the surfaces. In: *Proceedings of the Canadian Geotechnical Conference*, Halifax, Nova Scotia, pp 253–262
- Gerrard C (1986) Shear failure of rock joints: appropriate constraints for empirical relations. *Int J Rock Mech Min* 23(6):421–429
- Ghazvinian A, Azinfar M, Vaneghi RG (2012) Importance of tensile strength on the shear behavior of discontinuities. *Rock Mech Rock Eng* 45(3):349–359
- Grasselli G, Egger P (2003) Constitutive law for the shear strength of rock joints based on three-dimensional surface parameters. *Int J Rock Mech Min* 40(1):25–40
- ISRM (1978) Commission on standardization of laboratory and field tests of the international society for rock mechanics: 'suggested methods for the quantitative description of discontinuities'. *Int J Rock Mech Min* 15(6):320–368
- Jing L, Nordlund E, Stephansson O (1992) An experimental study on the anisotropy and stress-dependency of the strength and deformability of rock joints. *Int J Rock Mech Min* 29(6):535–542
- Ladanyi B, Archambault G (1969) Simulation of shear behaviour of a jointed rock mass. In: *Proceedings of the 11th US Symposium on Rock Mechanics (USRMS)*, Berkeley, California, pp 105–125
- Lee H, Park Y, Cho T, You K (2001) Influence of asperity degradation on the mechanical behavior of rough rock joints under cyclic shear loading. *Int J Rock Mech Min* 38(7):967–980
- Leong E, Randolph M (1992) A model for rock interfacial behaviour. *Rock Mech Rock Eng* 25(3):187–206
- Li Y (2016) A constitutive model of opened rock joints in the field. Ph.D. thesis, University of New South Wales, Sydney
- Li Y, Oh J, Mitra R, Hebblewhite B (2016) A constitutive model for a laboratory rock joint with multi-scale asperity degradation. *Comput Geotech* 72:143–151
- Li Y, Oh J, Mitra R, Canbulat I (2017) A fractal model for the shear behaviour of large-scale opened rock joints. *Rock Mech Rock Eng* 50(1):67–79
- Li Y, Wu W, Li B (2018) An analytical model for the shear behaviour of rock joints under constant normal stiffness conditions. *Rock Mech Rock Eng* 51(5):1431–1445
- Oh J, Cording E, Moon T (2015) A joint shear model incorporating small-scale and large-scale irregularities. *Int J Rock Mech Min* 76:78–87
- Patton F (1966) Multiple modes of shear failure in rock. In: *Proceedings of the 1st ISRM Congress*, Lisbon, Portugal, pp 509–513
- Plesha M (1987) Constitutive models for rock discontinuities with dilatancy and surface degradation. *Int J Numer Anal Met* 11(4):345–362
- Queener C, Smith T, Mitchell W (1965) Transient wear of machine parts. *Wear* 8(5):391–400
- Saeb S, Amadei B (1992) Modelling rock joints under shear and normal loading. *Int J Rock Mech Min* 29(3):267–278
- Schneider H (1976) The friction and deformation behaviour of rock joints. *Rock Mech* 8(3):169–184
- Wong T, Baud P (2012) The brittle-ductile transition in porous rock: a review. *J Struct Geol* 44(2012):25–53
- Yang Z, Di C, Yen K (2001) The effect of asperity order on the roughness of rock joints. *Int J Rock Mech Min* 38(5):745–752
- Zou L, Jing L, Cvetkovic V (2015) Roughness decomposition and non-linear fluid flow in a single rock fracture. *Int J Rock Mech Min* 75:102–118

**Publisher's Note** Springer Nature remains neutral with regard to jurisdictional claims in published maps and institutional affiliations.